Fibers and Polymers 2022, Vol.23, No.3, 807-818
DOI 10.1007/s12221-022-3151-2

ISSN 1229-9197 (print version)
ISSN 1875-0052 (electronic version)

Accelerated Aging Effect in Physical and Thermo-mechanical Properties of Maize Starch Biocomposites Reinforced with *Agave Salmiana* Fibers from Different Leaf Ages

Alicia Reyes Samilpa[1], Diana P. Ferreira[2], Marta A. Teixeira[2], Raul Fangueiro[2,3], and Miguel C. Gutiérrez[4]*

[1]*Instituto Politécnico Nacional, CIIDIR Oaxaca. Hornos 1003, Col. Noche Buena, Santa Cruz Xoxocotlán, C.P.71230, Oaxaca, México*
[2]*Centre for Textile Science and Technology (2C2T), University of Minho, 4800 Guimarães, Portugal*
[3]*Department of Mechanical Engineering, University of Minho, 4800 Guimarães, Portugal*
[4]*CONACYT - Instituto Politécnico Nacional, CIIDIR Oaxaca. Hornos 1003, Col. Noche Buena, Santa Cruz Xoxocotlán, C.P.71230, Oaxaca, México*

(Received September 28, 2020; Revised April 4, 2021; Accepted April 15, 2021)

Abstract: In this study, lignocellulosic fibers from *Agave salmiana* –an important socio-economical species endemic to Mexico– were used to reinforce thermoplastic maize starch (TPS). Fibers from young raw leaves (YRL) and old roasted leaves (ORL) were obtained according to the traditional methods used by small producers. The formulations of biocomposites were obtained varying the content of both types of fiber and processed by extrusion and injection molding. Morphological, structural, mechanical, thermal, and thermomechanical properties of biocomposites were evaluated. To use the hydrophilicity of these materials as an advantage in unexplored applications, biocomposites behavior under degradative tests such as accelerated aging and salt water immersion was evaluated. The processes of heating the old leaves partially removed the lignin and hemicellulose layer from the fibers, which led to a better interaction fiber-matrix, as confirmed by FESEM, ATR-FTIR, and TGA. Biocomposites with 30 wt% of YRL fiber reported the highest values of tensile strength and Young's modulus when compared to ORL biocomposites and with TPS. Accelerated aging exposure affected mainly the thermomechanical properties of TPS and confirmed the reinforcing effect of the fibers due to the thermal and mechanical stability they provided to the matrix, especially when 20 wt% of fiber was added. This was also observed when biocomposites were immersed in salt water solution. Using *Agave salmiana* fiber obtained from different leaf ages by traditional methods in the production of biocomposites promotes the complete harnessing of this species and represents a possibility to small producers in Mexico to introduce circular economy in their communities.

Keywords: Thermoplastic starch, Hard fiber, Biocomposites, Extrusion-injection molding, Accelerated weathering

Introduction

The environmental problems caused by the disposal of large volumes of plastics, along with the depletion of petroleum stocks, have prompted an increasing interest in the design of new environment-friendly materials [1]. The use of raw materials from renewable natural resources and from agro-wastes promotes the use of green composites [2].

Poly(lactic acid), rubber, soy protein, and starch are polymers used as an alternative to the production of composites based on non-biodegradable materials [3]. Starch is a polysaccharide with thermoplastic behavior when water or glycerol is added under shear forces and continuous heat [4]. This polysaccharide can be obtained from cassava, maize, potato, among others, and has been widely studied and used as a polymeric matrix in the production of biocomposites [5-7] because of its low cost and availability [8].

The addition of natural fibers to thermoplastic starch increases its mechanical properties and thermal stability [9]. Plant fibers present several advantages over synthetic fibers, such as abundance, renewability, sustainability, biodegradability, low density or lightness, high specific properties, and low production costs [3,5]. Fiber with low lignin and hemicellulose content on the surface creates a strong interfacial bonding, improving the response of biocomposites to accelerated aging, as observed by Islam *et al*. [10] in PLA reinforced with alkali-treated hemp fibers. The accelerated aging technique is used to reproduce the weathering effects on materials exposed to sunlight, moisture, or dew, under controlled conditions on laboratory accelerated exposure devices [11].

Hard fibers can be obtained from the leaves of different agave species and represent a significant source for textile and artisan products. The most commercial agave species used to obtain hard fibers used to reinforce different polymers, mainly polyolefins, are sisal (*Agave sisalana*) [2,12-14], henequen (*A. fourcroydes*) [15-17], and fiber from *A. americana* [18-20]. Other studies have evaluated the fibers from by-products –mostly bagasse– of the tequila (*A. tequilana*) production as reinforcing material [21,22].

Another socio-economical relevant agave species in Mexico is *A. salmiana*, which is endemic to Mexico and widely distributed over the country [23], especially in arid and semi-arid zones of the north-central region [24,25], with poor soil conditions [26], and is potentially resistant to

*Corresponding author: michavezg@ipn.mx

climate change [27]. The major economic relevance of this species is the production of the distilled "mezcal" and fermented "pulque" beverages [25-28]. To obtain these products only the core of the agave plant is harnessed and the leaves –with different stages of maturity– are discarded [28], left in the fields [26], and considered an agro-industrial waste in several regions of the country [9].

In a smaller productive scale the leaves with different maturity stages of *A. salmiana* represent a source to obtain high-quality textile fiber, which is an important economic activity for artisan producers and their families, especially in one region of central Mexico named the Mezquital Valley, Hidalgo [29], and occasionally in some localities of Jalisco and Mexico City [25]. These fibers are obtained only by artisanal methods, which vary depending on the age of the leaf: when young leaves are used, they are manually scraped at raw to obtain the fiber, and when mature and old leaves are used, a roasting process is applied to the leaves prior the manual scraping process. The use of these fibers in industries different from textiles represents an opportunity to small producers to initiate circular economy in their communities.

As mentioned, the leaf fiber of *A. salmiana* is barely known at large productive scale and has not been reported as a reinforcing agent for composite materials. Therefore, the aim of this work was to evaluate *A. salmiana* fibers obtained by two traditional methods, according to the age of the leaf, as the reinforcing phase in biocomposites based on thermoplastic maize starch. Biocomposites were exposed to two types of degradative tests: the first was an accelerated aging technique and the second a long immersion test in salt water, to observe their degradation behavior in different environmental contexts and to use their hydrophilic nature as an advantage in unexplored, short-live, biodegradable applications, such as the design of artificial substrate tiles for coral reef restoration, given that the materials currently used are contaminant as the concrete or petroleum based plastics [30].

Experimental

Materials

Agave salmiana var. *Xa'mni* fiber was obtained by traditional method from the Mezquital Valley, Hidalgo, Mexico. Leaves with two different maturity stages were used to obtain the fiber: young leaves (3-4 years), and old leaves (around 8 years). Maize starch was supplied by Sigma-Aldrich, and glycerol was purchased from ACS Fermont. In order to remove parenchyma remnants from the fiber, washing powder (with linear alkylbenzene sulfonate as active ingredient and proteolytic enzyme), sugarcane white vinegar (with 5 % acidity), and tap water were used. Purified drinking water was used to moisten the maize starch.

Obtaining and Processing the *Agave Salmiana* Fibers

The first stage of the traditional process is to obtain the agave fiber from young leaves by manual scraping. This technique consists in separating the fiber beams from the parenchymal tissue of the leaf by beating the base of each leaf with a wooden mallet. Then, the agave leaf is pressed against a wooden board fixed in the soil with a wooden rod knife, scraping with up-and-down movements to remove the fibers from the parenchymal tissue.

As old leaves contain a higher amount of parenchymal tissue, they are roasted in a domestic wood fire at up to 400 ^{o}C to soften and moisten them to easily remove the fiber [31-33]. After this process, the leaves remained covered with a cotton blanket for three days, and then, the fiber was obtained by manual scraping.

Fiber Processing

To soften YRL fibers, they were immersed in a solution of 1:2:20, detergent, sugarcane white vinegar, and tap water, for 5 hours or overnight, depending on the time elapsed since the scraping process. In contrast, ORL fibers were soaked for three days in a mix of 1:10, corn meal and tap water. Afterwards, both YRL and ORL fibers were rinsed, drained and dried under an outdoor shade. Then, to remove minor fibers and particle traces, the fibers were carded.

After the preparation process, fibers were cut into segments of 2 cm long and then milled in a Fritsch Cutting Mill Pulverisette 19 (Idar-Oberstein, Germany) –with tungsten V blades– using 250 μm sieves. Then, these short fibers were passed through three W. S. Tyler ASTM E-11 stainless steel sieves (No. 200, 100, and 50) to obtain a length range within 75±5 μm to 300±14 μm. Finally, the resulting fibers were placed in 10×15 cm aluminum foil trays and dried in an oven (Arsa AR-290D, Jalisco, México) at 60 °C±2 °C for 24 h.

Biocomposite Production

To produce the biocomposites, 10, 20, and 30 wt% of YRL and ORL fiber contents were separately added (Table 1) to the maize starch that was previously moisturized with 20 % of purified water, manually stirred for 10 minutes, and rested for 24 h in hermetically sealed plastic bags. Then, 20 % of glycerol was added to each formulation and manually stirred for 10 minutes before extrusion. Thermoplastic maize starch (TPS) without fiber was used as control material. After this, the extrusion and injection processes were performed. The extrusion was carried out in a DSM Xplore MC-5 micro compounder (Geleen, Netherlands) with double conical screw with the following parameters: 90 °C at the three heating zones of the barrel; screw rotation speed of 100 RPM at the feed and processing areas. The injection was performed in a micro injection moulder DSM Xplore IM 5.5 (Geleen, Netherlands) with the following parameters: 95 °C in the heating barrel, 35 °C in the injection mold with 10 bar of pressure. The dimensions of the samples were established according to the type V of the ASTM D638 Standard Test Method for Tensile Properties

Table 1. Experimental design of polymeric matrix and biocomposite formulations

Sample ID	Maize starch (wt%)	Water (wt%)	Glycerol (wt%)	ORL fiber (wt%)	YRL fiber (wt%)
TPS	60	20	20	-	-
TPS/YRL10	60	20	20	-	10
TPS/YRL20	60	20	20	-	20
TPS/YRL30	60	20	20	-	30
TPS/ORL10	60	20	20	10	-
TPS/ORL20	60	20	20	20	-
TPS/ORL30	60	20	20	30	-

of Plastics.

Morphological Analysis

The morphological surfaces of YRL and ORL fiber and biocomposites were analyzed by Field Emission Electron Microscopy (FESEM) using a NOVA 200 Nano SEM from the FEI Company (Oregon, USA) at 10 kV of acceleration voltage. Samples were fractured with liquid nitrogen on their transversal area and coated with a layer of Au/Pd film (20 nm thickness and 80:20 wt%). The magnification range was from 500 and 5000×.

Fourier Transform Infrared (ATR-FTIR) Spectroscopy

Spectra of the fibers and the composites were obtained using an IRAffinity-1S, SHIMADZU FTIR spectrophotometer (Kyoto, Japan) with an ATR accessory. ATR-FTIR spectra of the samples were recorded in the range of 4000-400 cm^{-1}, with 45 scans and at a spectral resolution of 8 cm^{-1}. Scale in the fiber spectra was normalized.

Thermogravimetric Analysis (TGA)

Thermogravimetric analysis (TGA) was performed on an STA 449 F3 from NETZSCH Q500 (Bavaria, Germany) using aluminum pans. The weight of the specimens was 5±2 mg. The TGA trace was obtained in a temperature range of 25-600 ºC, at a heating rate of 10 °C/min under a dynamic nitrogen atmosphere with a flow rate of 10 m*l*/min.

Thermomechanical Analysis (TMA)

Thermomechanical tests were performed in a TMA Q400 from TA Instruments (Delaware, USA). First, the equipment was calibrated under the ASTM E2113-04 Standard Test Method for Length Change Calibration of Thermomechanical Analyzers. Samples were prepared according to the ASTM E 831-14 Standard Test Method for Linear Thermal Expansion of Solid Materials by Thermomechanical Analysis. To calculate the coefficient of thermal expansion (CTE) and glass transition temperature (Tg), the TMA was adjusted to the macro-expansion mode with an applied force of 0.02 N, and a temperature ramp from 0 °C to 100 °C with a rate speed of 5 °C/min. Samples were heated from 5 °C to 41 °C to calculate their CTE and to observe their behavior in a temperature of 23 °C±5 °C. Once obtained the curve of temperatures, the onset, midpoint, and endpoint temperatures of the Tg transitions were calculated using the tangents drawn on the displacement curve, considering the midpoint as Tg.

Mechanical Characterization

Tensile tests were performed using a Universal Testing Machine HOUNSFIELD H10KS (Surrey, UK) at room temperature (25 °C) with a constant speed of 5 mm/min, a load range of 50 N, an extension range of 50 mm, and a gauge length of 40 mm. The tests were performed according to ASTM D638.

Accelerated Aging

This experiment was conducted in an accelerated weathering tester QUV/spray from Q-Lab (Arizona, USA). Samples were exposed to a period of 500 h, as reported by Islam *et al*. [10], with 12 h of alternated condensation and UV radiation cycles. The condensation cycle was performed for 4 h at 50 °C using laboratory distilled water, while the irradiation cycle was for 8 h at 60 °C. An Ultra-Violet A [UVA] 340 lamp at 0.76 W/m^2 was used for irradiation exposure.

Immersion Test

The ASTM D570-98 Standard Test Method for Water Absorption of Plastics was performed to evaluate the behavior of the biocomposites immersed in salt water. For this test, three samples of 9.7×9.7±0.1 mm from each formulation were used. A salt water solution was prepared with 1000 m*l* of distilled water, 33.3 g of NaCl and 0.1 m*l* of NaOH to simulate seawater conditions of 33 ppm of salinity and 8.2 pH [34]. Each sample was placed in a 20 m*l* glass vial completely covered with the salt water solution for 30 days, following the step 7.4 Long Term Immersion of the ASTM D570-98.

In order to evaluate the best performance among the biocomposites, a Generalized Linear Model (GLM) with a Least Significant Difference (LSD) Fisher test was recorded. Then, to predict the behavior of the biocomposites during a longer period of immersion, a Linear Regression Model was performed. Statistical analysis were done in InfoStat [35].

Results and Discussion

Morphological Analysis

FESEM images of YRL and ORL are shown in Figure 1 at different magnifications to analyze and compare their surface morphology. Typical properties of hard agave fibers are observed in Figure 1(a), 1(c), 1(f), and 1(h), including the

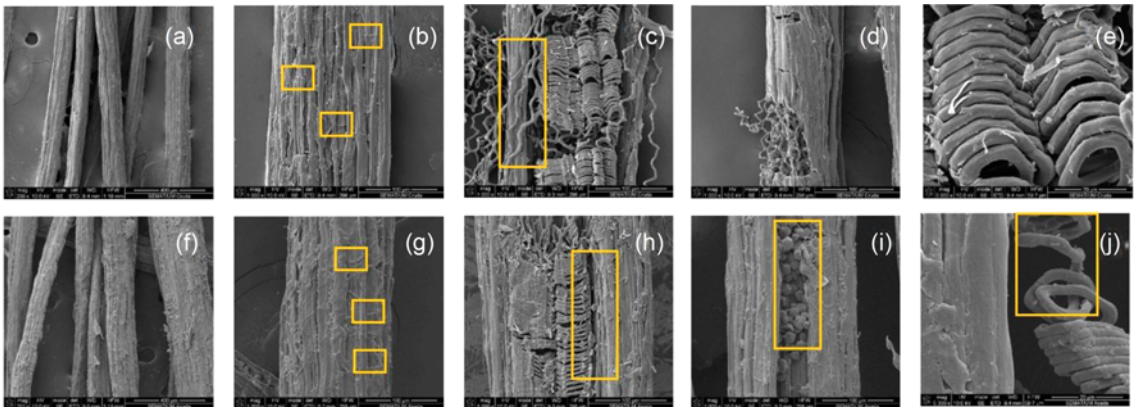

Figure 1. FESEM images of *Agave salmiana* fibers with different magnifications. From (a) to (e): YRL fiber; from (f) to (j): ORL fiber.

cementing substances lignin, hemicellulose and pectin that hold together the elementary fibers or cellulose microfibers; cellulose helicoidally arranged chains (Figure 1(c), 1(d), 1(e), 1(h) and 1(j)) as observed by John and Thomas [36]; and lines located along the fibers (Figure 1(b) and Figure 1(g)), distinctive to long lignocellulosic fibers [37].

Some residual fats or waxes remain in the fiber after the extraction process, especially if no chemical treatment has been carried out, due to the fiber beam containing some of these particles, as can be seen in Figure 1(i). This was also observed by Bismarck *et al*. [38]. They found small particles attached in the granular surface of raw *Agave sisalana* fibers, possibly waxy and fatty substances not soluble in water without a previous treatment such as alkali [39].

Teli and Jadhav [40] stated that the mechanical process used to obtain *Agave angustifolia* fiber influences the layer of lignin and hemicellulose surrounding the cellulose microfibrils, given that the retting extraction also involves a chemical process. This suggests that, in addition to the maturity effect of the fibers, the differences between ORL and YRL fiber observed in their morphological surface, such as an apparent thicker layer of lignin (Figure 1(g)) and the presence of residues (Figure 1(i)) in ORL fiber, could be attributed to the washing treatment YRL fiber received after the scraping process, resulting in a slimmer and more defined layer of lignin and hemicellulose covering the cellulose microfibrils (1(b)).

In Figure 2 the fiber-matrix interface is shown. A homogeneous interaction fiber-matrix was obtained, especially with 20 and 30 wt% of YRL content (Figure 2(b) and 2(c)). Some fractures appeared in the matrix, possibly as an effect of liquid nitrogen fracturing (Figure 2(g) and 2(j)). Micrographs with 5000× magnification show that the presence of lignin and hemicellulose impairs the interaction fiber-matrix, by creating micro-pores in the fiber (Figure 2(l)), as stated by Sreekala *et al*. [41]. The pull-out effect is more evident in TPS/ORL30 biocomposite (Figure 2(i)). This indicates a lower interaction fiber-matrix if compared with all TPS/YRL biocomposites, where gaps surrounding the YRL fiber are smaller and less frequent.

Fourier Transform Infrared (ATR-FTIR) Spectroscopy

In Figure 3 the spectra of YRL and ORL are shown. In general, a broad and well defined band at 3300 cm^{-1} is related to the hydroxyl group stretching vibration typical of polysaccharides such as cellulose, lignin and hemicellulose [42,43]. This band can also be attributed to inter- and intra-molecular hydrogen bonds of the cellulose [40,44,45]. Although a significant change in length or definition between the bands of the two types of fiber was not observable, the signal for YRL was found at 3332 cm^{-1} while in ORL shifted to 3279 cm^{-1}. According to the study made by Poletto *et al*. [45] of four different wood fibers the shifting to lower values suggests an increase in strength of the hydrogen-bonding, specifically within the frequency of 3432-3277 cm^{-1} which corresponds to inter and intramolecular changes in the H-bonds contained in cellulose. One possible explanation could be that the roasting pretreatment applied to ORL fibers might have affected the consistency of the lignin and hemicellulose matrix, leading to stronger H-bonds on their cellulose chains if compared to YRL fibers.

All the following signals appeared in both YRL and ORL fibers. The band at 2920 cm^{-1} is generally associated with the asymmetrical C-H stretching vibration of cellulose and hemicellulose [42]. At 1728 cm^{-1}, the stretching vibration of the internal double bonds in C=O from hemicellulose, lignin, pectin, and waxes appeared [40,42,46-48]. The aromatic C=C stretching bonds typical of lignin are observed at 1604 cm^{-1} [40] and at 1507 cm^{-1} [42].

The band at 1424 cm^{-1} corresponds to the in-plain bending HCH,OCH vibration of the cellulose [42], and it can be associated to its crystalline structure [44] and to aromatic skeletal vibrations [49]. However, if the band is close to 1460 cm^{-1}, it is attributed to the bending and stretching of C-H and C-O groups, respectively, present in lignin and carbohydrates of the fiber [50]. The signal at 1368 cm^{-1} is

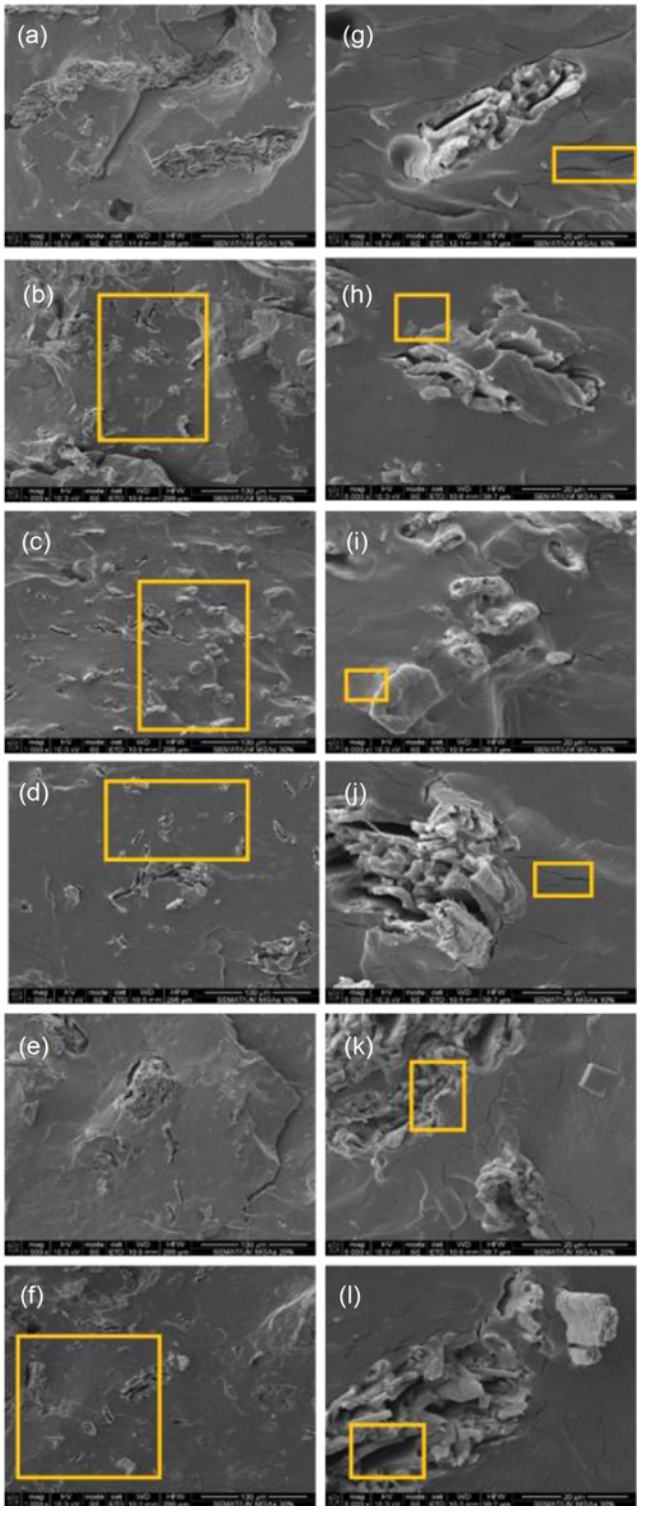

Figure 2. Micrographs of the fiber-matrix interface obtained by FESEM. Left column at 1000× magnification, right column at 5000× magnification. (a) and (g) TPS/YRL10, (b) and (h) TPS/YRL20, (c) and (i) TPS/YRL30; (d) and (j) TPS/ORL10, (e) and (k) TPS/ORL20, and (f) and (l) TPS/ORL30.

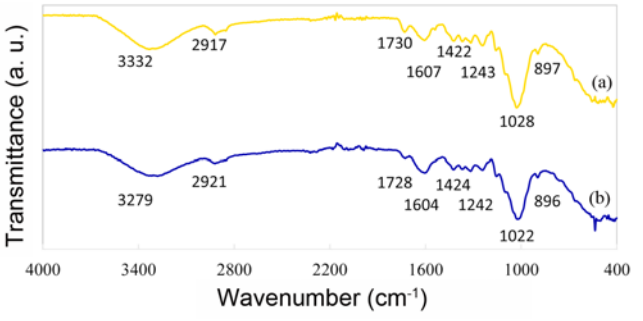

Figure 3. ATR-FTIR spectra of *Agave salmiana* var *Xa'mni* fibers; (a) YRL fiber and (b) ORL fiber.

related to the CH in-plain bending vibration of the cellulose and hemicellulose [42].

The rocking vibration of CH_2 of the cellulose can be observed at 1317 cm^{-1} [42].

At 1243 cm^{-1}, symmetric stretching of C=O and G (guaiacyl) ring of lignin [42,49]. At around 1020 and 1030 cm^{-1}, a wide peak corresponding to the symmetric C-O stretching of lignin appears [51]. Peaks found at 897 and 896 cm^{-1} are attributed to β-glucoside linkage of cellulose and hemicellulose [46]; these peaks are also related to the amorphous region in cellulose [44].

In spite Dai and Fan [42] and Hospodarova *et al*. [44] stated that signal at 1603 cm^{-1} shifting up to 1623-1633 cm^{-1} is related to the OH bend of absorbed water in cellulose, this was not the case for either of the fibers. Given the old leaves were roasted, the esters of the fibers were hydrolyzed and broke down into acids and alcohols decreasing the content of lignin and hemicellulose that covers the cellulose microfibrils of ORL fiber. Hydroxyl groups of the cellulose crystalline region create hydrogen bonds with parallel chains, reducing the absorption of water [41], as observed in ORL fiber with the cellulose microfibrils more exposed than in YRL fiber.

In Fogure 4 typical signals of thermoplastic starch can be observed. The strong broad band at 3286 cm^{-1} is attributed to the stretching vibration of hydroxyl groups derived from the hydrogen bonding of starch [52,5]. The signal at 2927 cm^{-1} corresponds to the C-H stretching and at 1649 cm^{-1} it is associated to bound water [52], which is consistent with the hydrophilic nature of starch. The bending vibration of C-H and C-O typical of aromatic rings was observed at 1338 cm^{-1} [53]. The band found at 1417 cm^{-1} is attributed to the presence of glycerol in the material [52]. At 1149 cm^{-1}, the C-O stretching of typical functional groups of starch and glycerol were found. The C-O bending vibration at 1078 cm^{-1} suggests a strong hydrogen bonding interaction of OH groups [53,54], and the O-C stretching of anhydroglucose ring occurred at 995 cm^{-1} [5].

For biocomposites, a variation in the intensity of signals

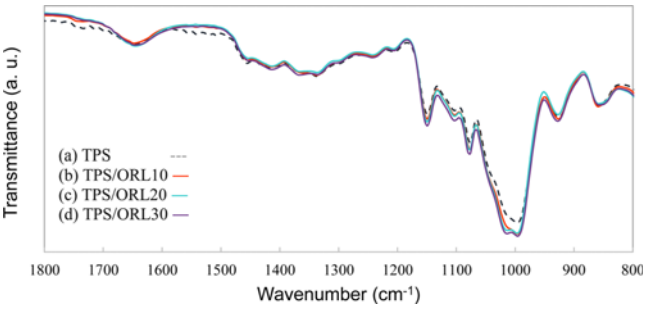

Figure 4. ATR-FTIR spectra of thermoplastic maize starch and biocomposites reinforced with 10, 20, and 30 wt% of old leaf fiber before accelerated weathering: TPS (a); TPS/ORL10 (b); TPS/ORL20 (c); TPS/ORL30 (d). (For interpretation of the references to colour in this figure legend, the reader is referred to the web version of this article.)

related to lignin at 1730 and 1245 cm^{-1} was expected to be observed as the content of the fiber increased or as different fiber age was used. However, all the signals of aromatic rings typical of lignin completely overlapped with the functional groups of starch.

All the biocomposites spectra (Figure 4) exhibited an absorption band in the range of 3300 cm^{-1}, which can be attributed to different modes of stretching of the O-H bond, typical of the cellulose structure, and a slight shift occurred if compared with TPS. The presence of the two absorption bands at 2920 and 2850 cm^{-1} may be caused by the presence of pectin, waxes, and esters containing methyl and methylene groups. The bands at 1240 and 1160 cm^{-1}, as well as the bands at 1020 cm^{-1}, can be assigned to C=O, C-H, C-O-C, and C-O deformation or the stretching of the vibrations of different groups in the carbohydrates. A peak near 1100 cm^{-1} corresponds also to C-O-C stretching vibrations of cellulose [45,55]. A shift can be observed at 1078 cm^{-1} as the fiber content increases, which is an indicator of improved interaction between components [54].

The spectra of the biocomposites either before accelerated weathering or with 500 h of exposure display no shifting, which reveals their capacity to withstand UV radiation. Similarly, a peak at around 1730 cm^{-1} related to the stretching vibration of C=O proves the permanence of hemicellulose, lignin, and pectin even after accelerated weathering.

Thermogravimetric Analysis (TGA)

TGA curves of YRL and ORL are shown in Figure 5. The thermograms of the fibers showed that the drop in mass occurred in two stages: the first stage observed from the beginning of the test up to 90 and 85 °C for YRL and ORL fibers, respectively, corresponds to the loss of absorbed moisture –including chemisorbed water and/or intermolecularly H-bonded water [56] on the surface of both fibers. The difference in the degradation temperature of the fibers at this initial stage could be related to the results reported in section 3.2 concerning the H-bonding strength of the cellulose, which increased in ORL fibers as the frequency of their OH stretching band at around 3300 cm^{-1} decreased, according to the stipulated by Poletto *et al*. [45] in wood fibers.

The second stage of mass loss registered occurred from 180 °C to 380 °C. This can be attributed to the thermal decomposition of hemicellulose and the rupture of the glycoside link of the cellulose molecule [13]. The presence of a drop at around 270 °C in the thermogram of ORL fiber highlights the decomposition of the hemicellulose, which occurred in a range of 250-300 °C in an inert atmosphere [57]. This may reveal a non-uniform content of hemicellulose in the fiber caused by the pretreatment the fiber received. The mass loss observed as a flat tailing section of the TGA curve in the range of 350-500 °C is attributed to the degradation of lignin [57].

The firewood temperature in which the old leaves were roasted is unknown, since it was an artisanal process. However, a similar technique was described by Caballero *et*

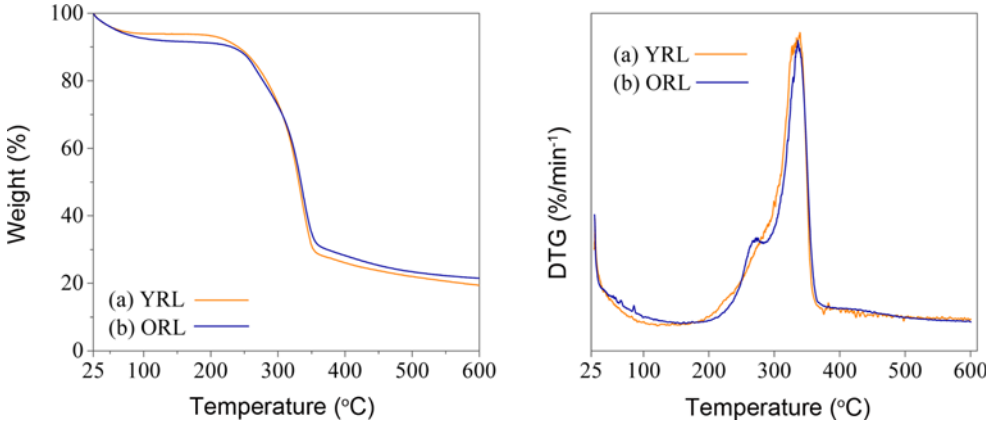

Figure 5. TGA (left) and DTG (right) curves of Agave salmiana fiber: (▬) YRL; (▬) ORL. (For interpretation of the references to colour in this figure legend, the reader is referred to the web version of this article.)

al. [33] to obtain fiber from the leaves of *Agave angustifolia* Haw. In their work, they cooked the leaves in a stone oven, and they observed that while the oven temperature reached up to 467 °C, leaves reached only up to 70 °C. The temperature reached by the leaves may explain why lignin –which degrades in a range from 200 to 700 °C [12]– was partially removed from ORL fibers.

TGA curves of TPS and biocomposites are shown in Figure 6. The thermal degradation curves of biocomposites indicate higher thermal resistance than those of neat fibers (Figure 5). The degradation of biocomposites occurs in two stages, the first one takes place at 230-380 °C and is associated with the degradation of non-cellulosic components (pectin and hemicelluloses), with the major component of fibers (cellulose), and the matrix. The second stage, with a slight slope at around 350-600 °C, is attributed to the degradation of lignin [55]. Biocomposites before accelerated aging exhibited a steep slope in their first loss, which occurred at 100 °C due to phased evaporation of absorbed and bound water in the matrix. This step was prolonged up to 200 °C where the migration of glycerol occurs [6].

The major mass loss occurred within 210-400 ºC for the different biocomposites. In comparison to the fiber thermograms (Figure 6), there was a decrease in the maximum degradation temperature due to the presence of thermoplastic starch. As a particular feature of plasticizers, glycerol changed the structure of the starch by breaking its intermolecular or intramolecular hydrogen bonds, increasing its plasticity by reducing the intermolecular interactions within the starch chains.

TPS/ORL biocomposites were closer to the stable behavior of TPS at the beginning of the thermo-degradation. However, at around 480 °C these biocomposites were more stable than TPS as an effect of the lignocellulosic content of fibers. By contrast, broader and steeper drops were observed for biocomposites with 500 h of accelerated weathering, particularly in TPS/ORL. This difference indicates that the UV radiation and simulated dew directly affected not only the plasticizers of the TPS, as observed in the first drop, but also the fibers, as shown in the final drop of TPS/ORL biocomposites, where temperatures corresponding to lignin degradation produced almost 15 % of mass loss.

The accelerated weathering exposure significantly affected the specimens of TPS, which started their physical deterioration before the 500 h of accelerated weathering. All the TPS specimens exhibited fractures in the grips area of the sample, and considerable bending in the testing area; therefore, thermogravimetric, thermomechanical, and mechanical characterization of this material was not performed because of the damages in the testing area. However, the addition of agave fiber to the TPS supports their performance as reinforcing material by improving the physical and mechanical properties of the polymeric matrix; hence, biocomposites with 500 h of accelerated weathering were able to be characterized.

The effect of plasticization, coupled with the degradation temperatures of glycerol at 213 °C and starch at 309 °C, increased the vulnerability of the biocomposites to the heat causing notable degradation of the matrix. This degradation was observed in the first peak of the TGA curves, with maximum degradation temperatures occurring at 300 ºC and 309 ºC for samples before accelerated weathering and with 500 h of accelerated weathering, respectively. Then, the

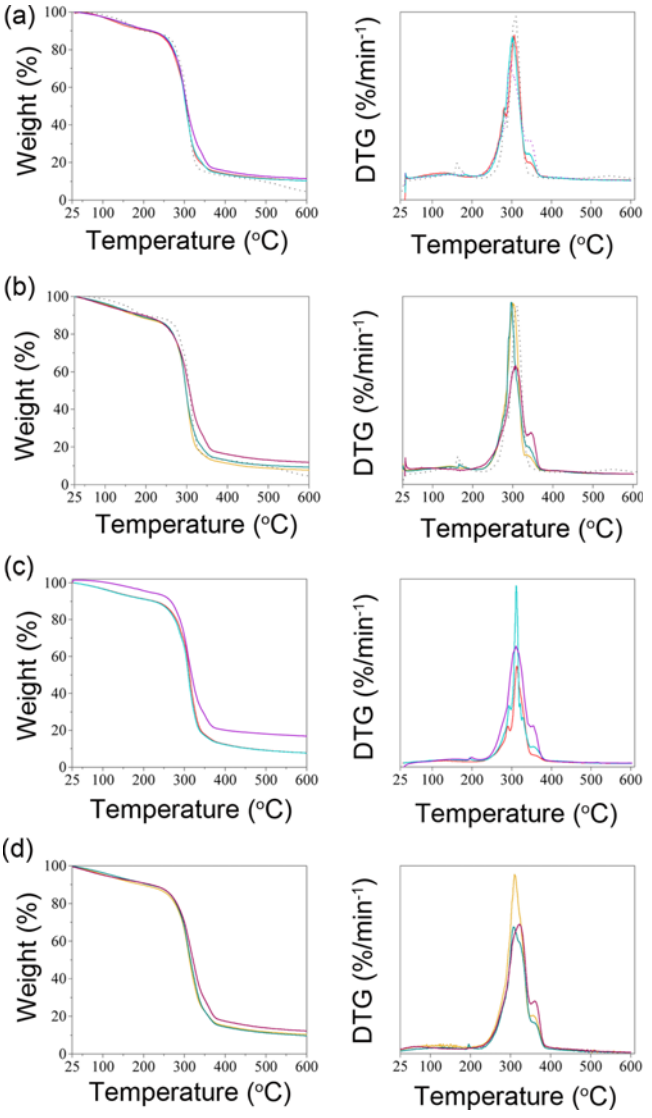

Figure 6. TGA and DTG curves of TPS and biocomposites; (a) TPS (- - -), TPS/ORL10 (—), TPS/ORL20 (—), TPS/ORL30 (—), (b) TPS (- - -), TPS/YRL10 (—), TPS/YRL20 (—), TPS/YRL30 (—), (c) accelerated aging effect on TPS/ORL10 (—), TPS/ORL20 (—), TPS/ORL30 (—), and (d) accelerated aging effect on TPS/YRL10 (—), TPS/YRL20 (—), TPS/YRL30 (—). (For interpretation of the references to colour in this figure legend, the reader is referred to the web version of this article.)

degradation of agave fibers was observed in the second peak at around 350 °C. Similar results were obtained by Islam *et al*. [10], who observed that fibers started to tear off from the eroding PLA matrix as an effect of the UV-radiation application.

This is consistent with the TGA curves that showed that increasing fiber content increases the thermal stability of thermoplastic maize starch, particularly in biocomposites containing 30 wt% of YRL fiber, which had a higher thermal resistance once the material burned off as illustrated in Fiugre 6.

Thermomechanical Analysis (TMA)

In Table 2 the thermomechanical properties variations of the biocomposites are observed regarding the type of the fiber (YRL and ORL), the content of the fiber (10, 20, and 30 wt%), and the accelerated weathering exposure time.

TPS samples registered a Tg of 48 ºC, which is in agreement with the temperature verified by Versino *et al*. [58]. This low value of Tg occurs since the function of the plasticizer is to increase the mobility of the polymer chains creating free volume [59]. Inversely, the incorporation of fiber increased the Tg of the polymeric matrix, indicating a good interaction fiber-matrix. This may be explained by the interaction between hydrophilic cellulose microfibrils –due to a low presence of lignin and hemicellulose in the fiber– and the absorbed water in the starch, allowing the migration of glycerol from the matrix to the fibers. The migration of water molecules also occurs when the small hydrophilic molecule of glycerol is inserted between the adjacent polymeric chains of the starch [60]. As observed by Gutiérrez *et al*. [61], increasing the filler decreases the chains mobility within the polymeric matrix, especially when treated fibers are added, since they exhibit stronger interfacial bonding when compared to pristine fibers. This effect is observed in biocomposites reinforced up to 20 wt% of both YRL and ORL fiber, possibly because the free volume can only be occupied at an optimum amount of reinforcing material, hence, adding a higher amount of fiber will decrease the molecular fiber-matrix interaction, as observed by Dorado *et al.* [62] in corn starch/silica nanocomposites.

In addition, the presence of the fibers affecting the thermal stability of the polymeric matrix can be observed in the CTE results. TPS and biocomposites with 10 and 20 wt% of fiber content exhibit slight changes in their thermal stability. However, a further increase (30 wt%) of YRL and ORL fibers decreased by 19 % and 33 % the CTE values, respectively, confirming the retaining effect on the polymeric chains expansion induced by the fiber. These differences are caused by the hydrogen bonds generated between the hydroxyl groups of the fiber and the TPS, which confirms a better interaction fiber-matrix in this biocomposite. This higher thermal dimensional stability of biocomposites was also observed by Gutiérrez *et al.* [61] when increasing curauá fibers content to reinforce cellulose acetate, particularly when fibers were chemically treated.

The degradation of the biocomposites exposed to 500 h of accelerated weathering was uneven, which probably interfered in the determination of thermomechanical properties, especially in TPS/ORL biocomposites, where the pattern of such properties is not as consistent as in TPS/YRL. After the exposure of biocomposites to cycles of UV radiation and moisture, Tg remained similar only in biocomposites reinforced with 20 and 30 wt% of YRL fiber, demonstrating a stable thermal dimension. By contrast, TPS/ORL biocomposites presented significant changes on the Tg values, particularly with 20 wt% of fiber. This result can be related to the heat treatment that old leaves received, providing the fiber a non-uniform surface as observed in FESEM and TGA, which, when compared to TPS/YRL bicomposites, showed a more stable thermal dimension behavior.

Finally, CTE values decreased in all samples exposed to accelerated aging, probably because the reduction in the polymeric chain size of the starch led to a degradation of the fibers exposed, hence, the fiber-matrix interface decreased. Changes in the moisture content of the polymeric matrix are caused by the swelling and shrinkage as the materials were exposed during the accelerated aging [10].

Table 2. Thermomechanical properties of TPS and biocomposites before accelerated weathering and with 500 h of accelerated aging. Glass transition temperature (Tg) and mean coefficient of thermal expansion (CTE mean, am) were calculated at 23 °C±5 °C

Sample	Before accelerated weathering		500 h accelerated weathering	
	Tg (±1 °C)	CTE mean, α_m (μm/(m·°C))	Tg (±1 °C)	CTE mean, α_m (μm/(m·°C))
TPS	48	102±3	nd	nd
TPS/YRL10	52	97±3	64	75±2
TPS/YRL20	69	109±3	68	75±2
TPS/YRL30	66	83±2	67	58±2
TPS/ORL10	57	110±3	82	78±2
TPS/ORL20	76	111±3	58	77±2
TPS/ORL30	64	69±2	73	79±2

nd=not determined.

Mechanical Characterization

In Figure 7 mechanical properties obtained by tensile tests of thermoplastic maize starch and biocomposites before accelerated weathering and with 500 h of accelerated weathering are shown.

The TPS samples reported the highest elongation value and the lowest tensile strength and Young's modulus compared to materials reinforced with fibers of *Agave salmiana*.

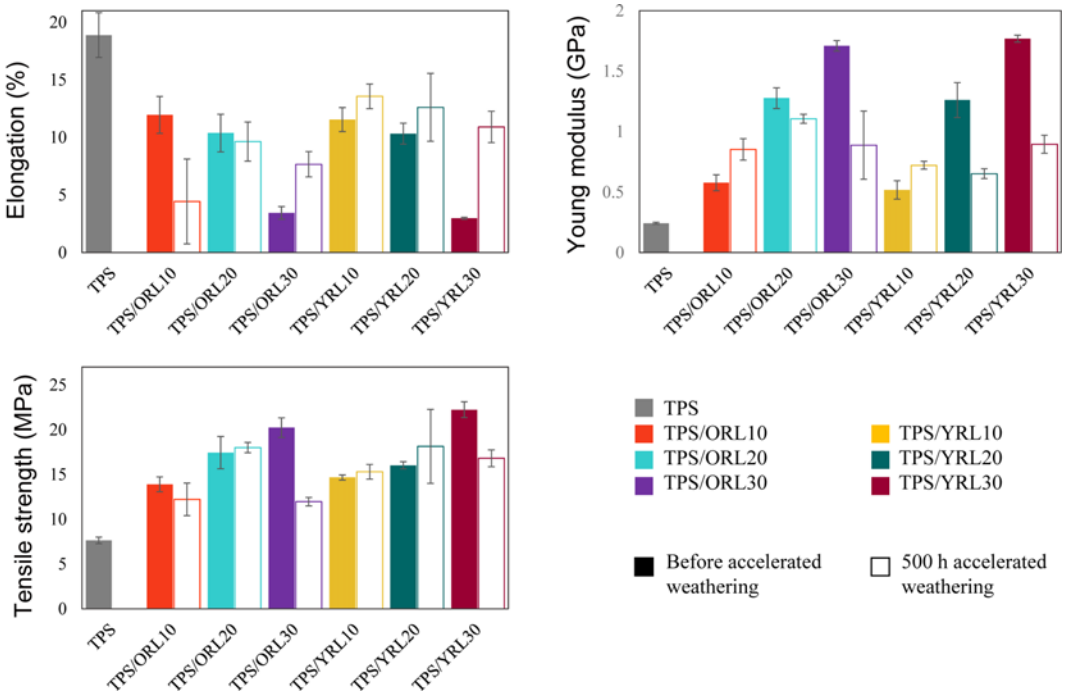

Figure 7. Mechanical properties of biocomposites with accelerated aging exposure. (For interpretation of the references to colour in this figure legend, the reader is referred to the web version of this article.)

The mechanical properties of biocomposites before accelerated weathering were not influenced by the type of fiber. However, there was an effect due to the content of fiber, at 10 and 20 wt% of both YRL and ORL fiber the elongation was similar, but it decreased when adding 30 wt%, which contributes to increase the mechanical strength of the TPS.

For biocomposites exposed to 500 h of accelerated weathering, an increase in elongation and decrease in tensile strength and modulus was observed, due to the migration of glycerol and the degradation of the fibers, as previously discussed in the thermomechanical and the ATR-FTIR analyses.

In general, the elongation decreases in samples before accelerated aging and increases in those exposed to 500 h. This can be attributed to the higher absorption of water by samples that registered higher degradation of fibers during the accelerated weathering, as observed by Islam *et al*. [10], providing a plasticizing effect. This is in agreement with the values of Tg obtained by thermomechanical analysis for TPS/YRL biocomposites. Also, the degradation of the fibers as an effect of the accelerated weathering exposure contributed to the decrease in the Young's modulus and the tensile strength of the biocomposites and to increase the elongation, which almost reached the original value of the TPS samples.

Immersion Test

In Table 3 the weight loss trend of TPS and biocomposites immersed in salt water is shown. As an effect of the long term immersion test, in all biocomposite samples the

Table 3. Weight loss in biocomposites by the effect of immersion in salt water

Sample	Mean weight (%)				
	Day 1	Day 7	Day 14	Day 21	Day 30
TPS	74.5±0.1	67.3±0.3	58.4±1.0	61.1±3.4	55.9±3.2
TPS/YRL10	80.6±11	69.2±1.1	63.3±4.9	61.9±7.6	54.9±7.1
TPS/YRL20	95.1±3.3	76.0±3.8	75.5±2.5	71.7±1.7	65.3±1.6
TPS/YRL30	129.1±0.2	74.9±4.8	74.3±10.6	53.8±10.7	42.1±17.3
TPS/ORL10	92.4±0.5	77.4±1.4	65.7±0.9	64.7±4.8	52.5±14.6
TPS/ORL20	76.1±1.3	67.7±2.7	59.7±2.4	58.6±2.0	50.4±2.6
TPS/ORL30	104.0±6	74.7±4.8	64.6±3.8	65.1±1.5	52.4±1.3

polymeric matrix was probably the first component dissolved in the water, because the remaining lignin in both types of fibers may inhibit the dissolution of the fibers in water during the time they were immersed. Even though hydroxyl groups can form hydrogen bonds between parallel chains and reduce water absorption [41], samples of biocomposites gained more weight when immersed in salt water if compared with samples of neat TPS, since both the polymeric matrix and the *Agave salmiana* fibers used are hydrophilic materials. Increasing the fiber content probably increases the porosity of the composites and the free volume for absorbing the salt water. This could be an effect of the mechanism of capillary through the microfractures present in the biocomposites surface, as reported by Sreekala *et al*. [41] in palm oil fiber reinforced composites.

A notable weight loss was recorded in TPS/ORL30 biocomposites, losing about 50 % of their initial weight. This result is in agreement with the FESEM images, where the surface of TPS/ORL30 presents protrusions, cracks, and pores that allowed a greater penetration of the water, dissolving the polymeric matrix with ease.

Therefore, biocomposites with 10 and 20 wt% of fiber content are in advantage when compared to further content of reinforcing material since its porosity may trigger the dissolution in water of the biocomposite.

Conclusion

The two types of *Agave salmiana* fiber used to reinforce thermoplastic maize starch led to slight differences in the properties of the biocomposites. The traditional method of heating the old leaves prior to the manual scraping process partially removed the layer of lignin and hemicellulose from the surface of the cellulose microfibrils, as observed in the micrographs of the fibers.

Different properties of thermoplastic maize starch improved when adding the two types of fibers. ORL fiber enhanced the tensile strength and the thermomechanical properties of thermoplastic maize starch when compared to YRL fiber biocomposites, probably because the heat applied to old leaves promoted a slight degradation of the lignin, triggering a good interaction between the hydroxyl groups of the cellulose and the TPS, decreasing the free volume in the interface of the ORL/TPS biocomposites.

By contrast, since YRL fibers were obtained by manual scraping at raw, the changes on their surface derived from mechanical damage only, leaving the layer of lignin and hemicellulose integrated. YRL fibers enhanced the properties of thermoplastic maize starch when subjected to accelerated weathering and salt water immersion, as observed in the thermal dimensional stability and mass stability, respectively.

The use of the two types of fibers evaluated as reinforcing phase in biocomposites is feasible and innovative, promotes the complete harnessing of residual leaves from the alcoholic beverages industry, and represents an opportunity for small producers in Mexico to develop circular economy.

Based on the results of the different tests performed, further uses of the biocomposites obtained in this study should consider the following: if a short time of processing the fibers is desirable, the use of YRL fibers is adequate; for applications demanding mechanical strength and thermal dimensional stability, formulations with 30 wt% of both fibers are recommended. In contrast, if the material is going to be exposed to sunlight, moisture, or dew, but structural mechanical properties are not required, YRL/TPS biocomposites are suitable. Finally, if the material is going to be immersed in conditions similar to marine environment, and considering approximately one month of material life under such conditions, the use of formulations with 20 wt% of both fibers is feasible.

Acknowledgements

A. Reyes-Samilpa acknowledges the scholarship 553944 from CONACYT; the mobility grant from CCA-IPN; the grants 251504 and 264110 from CONACYT, and 20195514 from SIP-IPN. We thank Dr. Edith Ariza from SEMAT Lab UMINHO and Dr. Ángel R. Hernández and M. C. Gerardo Fonseca from CFATA-UNAM for technical support in characterization tests; the Manuscript Writing Training Team (CEMAI in Spanish) of CONACyT for their help with reviews and constructive criticism, and Prof. Robert Leavitt and Maria del Sagrario Velasco García for also providing language help.

Electronic Supplementary Material (ESM) The online version of this article (doi: 10.1007/s12221-022-3151-2) contains supplementary material, which is available to authorized users.

References

1. M. P. Ho, H. Wang, L. Joong-Hee, C. K. Ho, K. T. Lau, J. Leng, and D. Hui, *Compos. Pt. B-Eng.,* **43**, 3549 (2012).
2. J. T. Kim and A. N. Netravali, *Compos. Pt. A-Appl. Sci. Manuf.,* **41**, 1245 (2010).
3. R. D. S. G. Campilho, "Natural Fiber Composites", 1st ed., pp.1-34, Tylor & Francis Group, CRC Press, Boca Raton, 2016.
4. L. Jiang and J. Zhang in "Handbook of Biopolymers and Biodegradable Plastics: Properties, Processing and Applications", 1st ed. (S. Ebnesajjad and W. Andrew Eds.), pp.109-128, Elsevier, Oxford, 2013.
5. A. Edhirej, S. M. Sapuan, M. Jawaid, and N. I. Zahari, *Int. J. Biol. Macromol.,* **101**, 75 (2017).
6. A. N. Frone, C. A. Nicolae, R. A. Gabor, and D. M. Panaitescu, *Polym. Degrad. Stabil*., **121**, 385 (2015).

7. N. Logié, G. Della Valle, A. Rolland-Sabaté, N. Descampse, and J. Soulestin, *Carbohydr. Polym.,* **184**, 57 (2018).
8. H. Angellier, S. Molina-Boisseau, P. Dole, and A. Dufresne, *Biomacromolecules,* **7**, 531 (2006).
9. G. H. Pulido, E. Hernández, V. M. Rabelero, R. R. J. Sanjuan, and G. C. F. Jasso, *Maderas-Cienc. Tecnol.,* **16**, 463 (2014).
10. M. S. Islam, K. L. Pickering, and N. J. Foreman, *Polym. Degrad. Stabil.,* **95**, 59 (2010).
11. ASTM, "G154-06", West Conshohocken, PA, 2006.
12. A. C. H. Barreto, D. S. Rosa, P. B. A. Fechine, and S. E. Mazzeto, *Compos. Pt. A-Appl. Sci. Manuf.,* **42**, 492 (2011).
13. B. Deepa, E. Abraham, N. Cordeiro, M. Mozetic, A. P. Mathew, K. Oksman, M. Faria, S. Thomas, and L. A. Pothan, *Cellulose,* **22**, 1075 (2015).
14. K. Senthilkumar, N. Saba, N. Rajini, Chandrasekar, M, Jawaid, M, S. Siengchin, and O. Y. Alotman, *Constr. Build. Mater.,* **174**, 713 (2018).
15. M. M. Rahman, *Mater. Des*., **30**, 2191 (2009).
16. A. May-Pat, A. Valadez-González, and P. J. Herrera-Franco, *Polym. Test.,* **32**, 1114 (2013).
17. D. Díaz-Batista, W. Saint Blancard-Valdés, V. Bridi-Tellez, M. Mazorra-Mestre, J. L. Valin-Rivera, F. R. Valenzuela-Díaz, and H. Wiebeck, *Rev. Cienc. Téc. Agropecu.,* **27**, 22 (2018).
18. K. Mylsamy, *Mater. Des.,* **32**, 4629 (2011).
19. A. S. Singha and R. K. Rana, *Mater. Des.,* **41**, 289 (2012).
20. D. D. Naidu, P. N. Mohan, B. P. C. Sekhar, M. T. Ahamad, and R. V. Prakash, *Int. J. Res. Appl. Sci. Eng. Technol.,* **5**, 2082 (2017).
21. S. Leduc, U. J. R. Galindo, R. González-Nuñez, Q. J. Ramos, B. Riedl, and D. Rodrigue, *Polym. Polym. Compos*., **16**, 115 (2008).
22. A. Santillán-Moreno, F. Martínez-Bustos, E. Castaño-Tostado, and S. L. Amaya-Llano, *Food Bioprocess Technol.,* **4**, 797 (2011).
23. M. Huerta-Lovera, C. B. Peña-Valdivia, A. García-Esteva, J. Kohashi-Shibata, H. Campos-García, and J. R. Aguirre-Rivera, *Genet. Resour. Crop Evol.,* **65**, 1649 (2018).
24. L. J. L. Mora, R.-A. J. A, J. L. Flores-Flores, V. C. B. Peña, and R. J. R. Aguirre, *Agrociencia,* **45**, 465 (2011).
25. I. Torres-García, F. J. Rendón-Sandoval, J. Blancas, A. Casas, and A. I. Moreno-Calles, *Bot. Sci.,* **97**, 263 (2019).
26. E. García-Moya, A. Romero-Manzanares, and P. S. Nobel, *Glob. Change Biol. Bioenergy*, **3**, 4 (2011).
27. M. Martinez-Salvador, R. Mata-González, C. Morales Nieto, and R. Valdez-Cepeda, *Environ. Manage.,* **49**, 55 (2012).
28. M. Láinez, H. A. Ruiz, A. A. Castro-Luna, and S. Martínez-Hernández, *Biomass Bioenerg.,* **118**, 133 (2018).
29. J. A. Reyes-Agüero, C. B. Peña-Valdivia, J. R. Aguirre-Rivera, and J. L. Mora-López, *Agrociencia,* **53**, 563 (2019).
30. R. E. Spieler, D. S. Gilliam, and R. L. Sherman, *Bull. Mar. Sci.,* **69**, 1013 (2001).
31. B. Aguilar-Juárez, J. R. Enríquez del Valle, G. Rodríguez-Ortíz, S. D. Granados, and C. B. Martínez, *Rev. Mex. Agroecosistemas*, **1**, 106 (2014).
32. G. L. Chávez, *Ingenierías,* **8**, 8 (2010).
33. C. M. Caballero, S. L. Silva, H. I. López, J. A. José, M. C. I. Crotés, B. J. L. Montes, and M. R. F. García, 14 Congreso Internacional Anual de la Sociedad Mexicana de Ingeniería Mecánica (SOMIM), Puebla, México, pp.89-94, 2008.
34. G. I. Retama, Ph. D. Dissertation, Instituto Politécnico Nacional, Ciudad de México, 2016.
35. J. Di Rienzo, F. Casanoves, M. G. Balzarini, L. Gonzáles, M. Tablada, and W. Robledo, InfoStat 2018, Universidad Nacional de Córdoba, Argentina, 2018.
36. M. J. John and S. Thomas, *Carbohydr. Polym.,* **71**, 343 (2008).
37. S. Msahli, J. E. Drean, and F. Sakli, *Text. Res. J.,* **75**, 540 (2005).
38. A. Bismarck, A. K. Mohanty, I. Aranberri-Askargorta, S. Czapla, M. Misra, G. Hinrichsen, and J. Springer, *Green Chem.,* **3**, 100 (2001).
39. A. K. Bledzki and J. Gassan, *Prog. Polym. Sci.,* **24**, 221 (1999).
40. M. D. Teli and A. Jadhav, *Am. Int. J. Res. Sci. Technol. Eng. Math.,* **17**, 6 (2017).
41. M. S. Sreekala, M. G. Kumaran, and S. Thomas, *Compos. Pt. A-Appl. Sci. Manuf.,* **33**, 763 (2002).
42. D. Dai and M. Fan, *Mater. Sci. Appl*., **1**, 336 (2010).
43. M. C. Gutiérrez, M. A. De Paoli, and M. I. Felisberti, *Compos. Pt. A-Appl. Sci. Manuf.,* **43**, 1338 (2012).
44. V. Hospodarova, E. Singovszka, and N. Stevulova, *Am. J. Anal. Chem.,* **9**, 303 (2018).
45. M. Poletto, A. J. Zattera, and R. M. C. Santana, *J. Appl. Polym. Sci.,* **126**, 336 (2012).
46. P. M. Bondaris, R. S. I. Y. Soenoko, and A. Purnowidodo, *J. Eng. Sci. Technol. Rev.,* **12**, 1399 (2017).
47. J. E. Carmona, T. K. Morales-Martínez, S. I. Mussatto, D. Castillo-Quiroz, and L. J. Ríos-González, *Rev. Mex.Cien. For.,* **8**, 100 (2017).
48. L. C. D. Naranjo, L. Alamilla-Beltrán, G. F. Gutiérrez-López, E. Terres-Rojas, J. Solorza-Feria, S. Romero-Vargas, H. T. Yee-Madeira, A. Flores-Morales, and R. Mora-Escobedo, *Rev. Mexicana Cienc. Agric.,* **7**, 31 (2017).
49. T. Rashid, C. Fai Kait, and T. Murugesan, *Procedia Eng.,* **148**, 1312 (2016).
50. C.-M. Popescu, G. Singurel, M.-C. Popescu, C. Vasile, and S. D. Argyropoulos, *Carbohydr. Polym.,* **77**, 851 (2009).
51. J. Jayaramudu, B. Guduri, and A. Varada Rajulu, *Carbohydr. Polym.,* **79**, 847 (2010).
52. J. F. Mendes, R. T. Paschoalin, V. B. Carmona, A. R. Sena Neto, A. C. P. Marques, J. M. Marconcini, L. H. C. Mattoso, E. S. Medeiros, and J. E. Oliveira, *Carbohydr. Polym.,* **137**, 452 (2016).
53. E. Syafri, A. Kasim, H. Abral, and A. Asben, *Int. J. Adv.*

Sci. Eng. Inf. Technol., **7**, 1950 (2017).
54. H. Tian, J. Yan, A. Varada Rajulu, A. Xiang, and X. Luo, *Int. J. Biol. Macromol.,* **96**, 518 (2017).
55. D. P. Ferreira, S. M. Costa, H. P. Felgueiras, and R. Fangueiro, *Key Eng. Mater.,* **812**, 66 (2019).
56. S. N. Monteiro, V. Calado, F. M. Margem, and R. J. S. Rodriguez, *J. Mater. Res. Technol*., **1**, 189 (2012).
57. M. Carrier, A. Loppinet-Serani, D. Denux, J.-M. Lasnier, F. Ham-Pichavant, F. Cansell, and C. Aymonier, *Biomass Bionergy,* **35**, 298 (2011).
58. F. Versino, O. V. Lopez, M. A. Garcia, and N. E. Zaritzky, *Starch/Stärke*, **68**, 1026 (2016).
59. R. A. de Graaf, A. P. Karman, and L. P. B. M. Janssen, *Starch/Stärke,* **55**, 80 (2003).
60. X. Chen, L. Guo, P. Chen, Y. Xu, H. Hao, and X. Du, *J. Cereal Sci.,* **77**, 135 (2017).
61. M. C. Gutiérrez, M. A. De Paoli, and M. I. Felisberti, *Ind. Crops Prod.,* **52**, 363 (2014).
62. A. Dorado, E. Peralta, E. Carpio, E. Lozada, and A. Elepaño, *Mater. Sci. Forum,* **894**, 66 (2017).